

Article

Isoscape of $\delta^{18}\text{O}$ in Precipitation of the Qinghai-Tibet Plateau: Assessment and Improvement

Yudong Shi ¹, Shengjie Wang ^{1,*} , Mingjun Zhang ¹, Athanassios A. Argiriou ² , Rong Guo ³,
Yang Song ¹ and Xiaofan Zhu ⁴

¹ College of Geography and Environmental Science, Northwest Normal University, Lanzhou 730070, China; syd_1995@126.com (Y.S.); mjzhang2004@163.com (M.Z.); sy5030.student@sina.com (Y.S.)

² Laboratory of Atmospheric Physics, Department of Physics, University of Patras, GR-265 00 Patras, Greece; athanarg@upatras.gr

³ Institute of Tibetan Plateau Research, Chinese Academy of Sciences, Beijing 100101, China; gsgrong@126.com

⁴ Northwest Institute of Eco-Environment and Resources, Chinese Academy of Sciences, Lanzhou 730000, China; zxf_jc@163.com

* Correspondence: geowang@126.com

Received: 6 November 2020; Accepted: 30 November 2020; Published: 2 December 2020



Abstract: The spatial distribution of stable water isotopes (also known as an isoscape) in precipitation has drawn increasing attention during the recent years. In this study, based on the observations at 32 stations, we assessed two widely applied global isoscape products (Regionalized Cluster-based Water Isotope Prediction (RCWIP) and Online Isotopes in Precipitation Calculator (OIPC)) at the Qinghai-Tibet Plateau (QTP) and then established an improved isoscape of oxygen isotopes in precipitation on a monthly basis using a regionalized fuzzy cluster method. Two fuzzy clusters can be determined, which is consistent using three meteorological data. The monthly isoscapes show the seasonal movement of high and low isotopic value regions across the QTP and reveal the influences of monsoon and westerly moisture. According to the cross validation, the $\delta^{18}\text{O}$ in precipitation in the new monthly isoscapes for the QTP we propose performs better compared to the existing global products. To create a regional isoscape in many other regions, the regionalized fuzzy cluster method can be considered especially for regions with complex controlling regimes of precipitation isotopes.

Keywords: precipitation; Qinghai-Tibet Plateau; $\delta^{18}\text{O}$, isoscape; fuzzy cluster

1. Introduction

The in situ monitoring of stable hydrogen and oxygen isotopes in precipitation provides a method to determine the hydrological processes at the global or regional scale [1,2]. As an important basis in isotope studies, the spatial distribution of hydrogen and oxygen stable isotopes in precipitation at different timescales has drawn more and more attention [3–6]. During the past decades, several elaborate methods have been used for isoscape mapping, and the global and regional isoscapes are helpful to understand the spatial regimes of precipitation isotopes [7–9].

For many hydrological and ecological researchers using stable isotope techniques, it is critical to know the distribution of long-term averages of stable water isotope ratios (especially in precipitation) on a monthly scale at least [10]. This need is covered by global or regional isoscape products with good resolution and accuracy. On a global basis, there are currently two sets of high spatial resolution products publicly available online, i.e., the Online Isotopes in Precipitation Calculator (OIPC; sometimes referred to as the BW model) [3,8,11] developed by Gabriel J. Bowen of the University of Utah, and the Regionalized Cluster-based Water Isotope Prediction (RCWIP) [12] developed by the International Atomic Energy Agency (IAEA). The data sources of these two products are mainly based on the

Global Network of Isotopes in Precipitation (GNIP) [13], although a small number of original data may have been obtained from other sources. Both products provide monthly and annual results and are spatially interpolated over the global land area using additional variables. Compared with other isotope products, they have a high resolution and can be obtained and used online.

In recent years, global isoscape products have been widely used in regional case studies. Especially in areas with limited or no data, the long-term mean of precipitation isotope ratios has been extracted from these products [4,14,15]. The global distribution of the GNIP stations is far from being uniform. In many low-populated regions, such as mountains, deserts, and glaciers, there is a lack of long-term time series of measured data. Isotope studies in these areas need complement data resulting from interpolation methods, and this introduces uncertainties. Consequently, the direct application of these global isoscape models to such an area without prior verification may lead to incorrect inferences.

The sources of precipitation and water vapor at the Qinghai-Tibet Plateau (QTP) are complex. According to Yao et al. [16], the QTP can be divided into three sub-regions regarding moisture regimes, namely the westerlies domain, the monsoon domain, and the transition domain. In the different parts of the QTP, aside from the different moisture sources, different local climate effects also exist. In the northwestern QTP, the altitude effect is significantly imprinted in the $\delta^{18}\text{O}$ of precipitation; moreover, the $\delta^{18}\text{O}$ values are remarkably correlated with surface air temperature [17]. At the Qinghai Lake watershed (in the northeastern QTP), precipitation isotopes are influenced by local moisture recycling [18]. Zhang et al. [19] found that at the central QTP $\delta^{18}\text{O}$ values show a significant seasonal variation. A positive correlation is shown between oxygen isotope values and temperature during the pre-monsoon and the westerlies season, and $\delta^{18}\text{O}$ is affected by regional convective activity during the monsoon season. At the southeastern QTP, regional precipitation is controlled by the monsoons; also, the moisture source changes with season [20]. Gao et al. [21] studied the $\delta^{18}\text{O}$ value in precipitation using two different isotope-equipped general circulation models (GCMs) in the southern part of QTP. The isotope-equipped GCM results are corrected using two types of spatial interpolation methods [22], in order to increase the accuracy of GCM-based results over the QTP. However, an updated isoscape with fine spatial resolution across the QTP is still needed for practical use.

It is clear that the QTP and its surrounding areas are poorly represented in the GNIP database since only a few stations such as Lhasa and Hotan contribute data to this database [7]. Consequently, an in-depth evaluation is required in order to check whether global precipitation isotope data products, including OIPC and RCWIP, can well depict the precipitation isotope information in the QTP. In this paper, we evaluate the applicability of the OIPC and RCWIP isoscapes in the QTP on a monthly scale using data published in literature. Furthermore, we propose a new isoscape for the QTP. This isoscape may provide a reference for further understanding the precipitation isotope mechanism and the regional hydrologic processes in the QTP under complex climate and environmental conditions.

2. Materials and Methods

2.1. Study Area and Isotope Observation Data

The Qinghai-Tibet Plateau, also known as the “roof of the world” and “water tower of Asia,” plays an important role in the current water cycle of Asia [23]. In this study, we focused on the plateau within the boundaries of China (Figure 1) [24]. In Figure 1a, the sub-region boundaries in the research scope are as follows: Qaidam (I), Eastern Qinghai-Tibet (II), South Tibet (III), Western Sichuan-Southeast Tibet (IV), Kunlun-Ngari-North Tibet (V), and South Himalayas (VI); the DEM (Digital Elevation Model) data are acquired from the Geospatial Data Cloud (<http://www.gscloud.cn>); the boundary of the QTP is based on Zhang et al. [24], and the division of sub-regions is according to Ren and Bao [25]. The long-term mean of precipitation amount (P) and air temperature (T) during 1981–2010 is provided by the China Meteorological Data Service Center (<http://data.cma.cn/>).

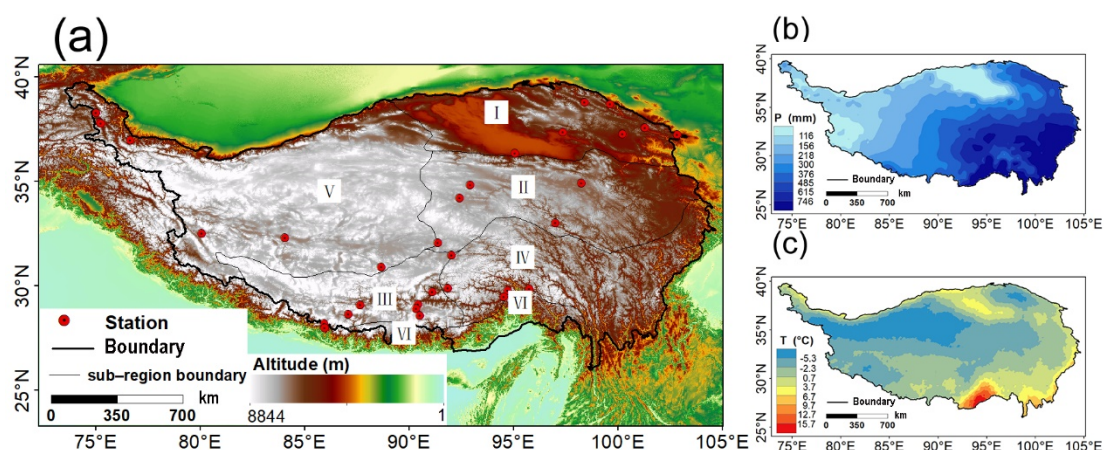


Figure 1. Maps showing sampling sites and altitude (a), long-term annual mean precipitation amount (b), and air temperature (c) in the Qinghai-Tibet Plateau (QTP).

The observed data used in this study were retrieved from the TNIP (the Tibetan Network for Isotopes in Precipitation) database [16] and other published papers (Table 1). For the isotopic data, we adopted strict data quality control standards: (1) The natural precipitation was collected without any direct impact of weather modification methods, and there was no artificial selectivity when collecting data; (2) The sampling duration was at least three months and the specific sampling date was provided; (3) Each sampling station operated independently; data could not be collected at multiple adjacent stations to form a single station data time series; detailed station information (e.g., latitude, longitude, and altitude) were available; (4) The data measurement error of $\delta^{18}\text{O}$ value was less than 0.5‰. Since precipitation in the QTP is not evenly distributed all year round, in this work, a year was divided into summer half year (May to September) and winter half year (October to April) [26]. Finally, this study collected 296 precipitation isotope data at 32 stations on a monthly scale.

Table 1. Basic information and long-term climatology for each sampling station across the Qinghai-Tibet Plateau.

Station	Longitude (°E)	Latitude (°N)	Altitude (m)	<i>P</i> (mm) ¹	<i>T</i> (°C) ¹	Water Vapor Regime ²	Sub-Region ³	<i>n</i> ⁴	Data Source
Tuole	98.42	38.80	3367	473	−5.35	the westerly domain	Qaidam	7	[27]
Yeniugou	99.63	38.70	3320	434	−0.55	the westerly domain	Qaidam	9	[28]
Haibei	101.31	37.56	3280	592	−0.89	the westerly domain	Qaidam	12	[29]
Delhi	97.37	37.37	2981	223	−0.29	the westerly domain	Qaidam	12	[16]
Gangca	100.22	37.29	3260	411	−0.31	the westerly domain	Qaidam	6	[30]
Tianzhu	102.85	37.25	2700	439	3.37	the westerly domain	Qaidam	10	[31]
Golmud	95.09	36.35	2889	63	3.01	the westerly domain	Qaidam	3	[32]
Muztag	75.02	38.28	4430	150	−0.84	the westerly domain	Kunlun-Ngari-North Tibet	5	[28]
Tizinafu	75.20	37.83	3058	96	0.10	the westerly domain	Kunlun-Ngari-North Tibet	4	[33]
Taxkorgen	75.27	37.77	3100	96	0.10	the westerly domain	Kunlun-Ngari-North Tibet	12	[16]
Xihexiu	76.68	36.98	2960	119	−2.90	the westerly domain	Kunlun-Ngari-North Tibet	10	[17]
Shiquanhe	80.08	32.50	4278	169	−2.18	the transition domain	Kunlun-Ngari-North Tibet	10	[16]
Gaize	84.07	32.30	4430	133	−1.81	the transition domain	Kunlun-Ngari-North Tibet	12	[16]
Xainza	88.70	30.90	4770	330	−1.25	the transition domain	Kunlun-Ngari-North Tibet	12	[19]
Madoi	98.26	34.92	4300	370	−3.69	the transition domain	Eastern Qinghai-Tibet	11	[34]
Beiluhe	92.94	34.83	4642	315	−4.81	the transition domain	Eastern Qinghai-Tibet	10	[35]
Tuotuohe	92.43	34.22	4533	323	−4.51	the transition domain	Eastern Qinghai-Tibet	12	[16]
Yushu	97.02	33.02	3682	656	−2.48	the transition domain	Eastern Qinghai-Tibet	12	[16]
Cona	91.40	32.07	4623	453	−2.06	the transition domain	Eastern Qinghai-Tibet	9	[36]
Lhasa	91.13	29.70	3649	426	1.62	the monsoon domain	South Tibet	12	[16]
Nagqu	92.07	31.48	4508	514	−1.95	the monsoon domain	South Tibet	12	[16]
Baidi	90.43	29.12	4430	358	0.25	the monsoon domain	South Tibet	11	[16]
Larzi	87.68	29.08	4000	336	0.69	the monsoon domain	South Tibet	4	[16]
Wengguo	90.35	28.90	4500	361	−0.43	the monsoon domain	South Tibet	7	[16]
Dingri	87.12	28.65	4330	302	−0.26	the monsoon domain	South Tibet	8	[16]
Dui	90.53	28.58	5030	389	−0.30	the monsoon domain	South Tibet	10	[16]
Nyalam	85.97	28.18	3810	396	−1.70	the monsoon domain	South Tibet	12	[16]
Zhangmu	85.98	27.98	2239	407	−1.64	the monsoon domain	South Tibet	4	[16]
Yangcun	91.88	29.88	3500	522	0.14	the monsoon domain	Western Sichuan-Southeast Tibet	8	[16]
Bomi	95.77	29.87	2737	553	3.12	the monsoon domain	Western Sichuan-Southeast Tibet	11	[16]
Lulang	94.73	29.77	3327	611	4.41	the monsoon domain	Western Sichuan-Southeast Tibet	11	[16]
Nuxia	94.57	29.47	2780	599	7.18	the monsoon domain	Western Sichuan-Southeast Tibet	8	[16]

¹ Annual mean precipitation amount (*P*) and air temperature (*T*) during 1981–2010 are provided by the China Meteorological Data Service Center (<http://data.cma.cn/>). ² The water vapor sources are classified according to Yao et al. [16]. ³ The division of sub-regions on the QTP according to Ren and Bao [25]. ⁴ To indicate the intra-annual coverages for each sampling site, the number is based on monthly counts from January to December, and the same month in different years is counted once.

2.2. Global Precipitation Isoscape

The isoscape OIPC v3.2 (available online at <http://wateriso.utah.edu/waterisotopes/>) is released by the University of Utah [11]; it provides monthly and annual $\delta^{18}\text{O}$ values. The spatial resolution used in this study was $5' \times 5'$. The OIPC uses measured isotope data as well as the latitude and altitude of known sampling stations in order to propose a best-fitting regression model:

$$\delta^{18}\text{O} = a|\text{LAT}|^2 + b|\text{LAT}| + c\text{ALT} + d \quad (1)$$

with $\delta^{18}\text{O}$ the predicted value, a , b , and c regression coefficients, d the intercept, LAT the latitude in degrees, and ALT the altitude in m. When the regression equation is determined, prediction by interpolation is performed using as auxiliary variables the latitude and altitude. Finally, the precipitation isotope estimates on a global scale are obtained by adjusting the predictions based on the residuals of each measured station.

The isoscape RCWIP v1.0 (http://www-naweb.iaea.org/naweb/ih/IHS_resources_rcwip.html) is a model with a resolution of $10' \times 10'$ developed by the IAEA [12]; compared to the OIPC, it includes more auxiliary variables especially meteorological parameters. Monthly and annual stable water isotope values are available online. Compared to the OIPC, the RCWIP does not adopt a unique global model, but calculates different regression models for each climate region through a fuzzy clustering method. This approach reduces the uncertainty of the global prediction model; furthermore, the clustering method makes the transition over boundaries smooth.

In this paper, ArcGIS10.2 was used to extract the simulated $\delta^{18}\text{O}$ values at the location of 32 measured stations in the QTP from the two global isoscapes and to evaluate their applicability in the study region.

2.3. Meteorological and Elevation Data

In order to produce a new isoscape over a region, meteorological data across this region are needed. To assess any eventual uncertainty introduced by the use of meteorological datasets, we tested three of them: (1) Dataset of monthly surface observation values in individual years in China compiled by the China Meteorological Administration (CMA); (2) Climatic Research Unit CL v2.0 dataset (CRU); (3) WorldClim v2.0 dataset (WC). Table 2 has more information about them. ArcGIS 10.2 was also used to extract the meteorological data at each sampling station. Regarding the meteorological input in predicting isoscapes over the QTP, the latitude and longitude range was extracted using a $0.5^\circ \times 0.5^\circ$ cell grid, resulting to a total of 999 grid points. A dataset was produced for CMA, CRU, and WC, respectively. The precipitation data were normalized using the natural logarithm function (setting 0 mm to be equal to 0.01 mm). In addition, the altitude values used in this paper come from the DEM data, provided by the Geospatial Data Cloud site, Computer Network Information Center, Chinese Academy of Sciences (<http://www.gscloud.cn>) with a 1 km resolution.

Table 2. Information about meteorological data.

	CMA	CRU	WC
Spatial Resolution	$30' \times 30'$	$10' \times 10'$	$10' \times 10'$
Period	1981–2010	1961–1990	1970–2000
Variable ¹	P, T	P, T	P, T, V
Reference	[37]	[38]	[39]
URL	http://data.cma.cn/	https://crudata.uea.ac.uk/cru/data/hrg/	http://worldclim.org

¹ P : precipitation amount; T : air temperature; V : water vapor pressure.

2.4. Fuzzy Clustering

A new $\delta^{18}\text{O}$ isoscape of the QTP was established by applying fuzzy clustering on the observed data. Fuzzy clustering partitions the study area according to meteorological parameters, allowing an

area to belong to multiple clusters but at a different degree; it avoids the impact of crisp partitioning on the results [12]. The Kaufman fuzzy clustering algorithm was used for calculation [40]. The algorithm seeks to minimize the objective function:

$$C = \sum_{k=1}^K \frac{\sum_{i=1}^N \sum_{j=1}^N m_{ik}^2 m_{jk}^2 d_{ij}}{2 \sum_{j=1}^N m_{jk}^2} \tag{2}$$

where m_{ik} is the unknown membership of the object i in cluster k , and d_{ij} is the dissimilarity between objects i and j . The memberships must be non-negative and the memberships of a single area or site, must sum to one.

In order to select the appropriate number of clusters empirically, we partitioned the area starting from 2 up to 15 clusters using each set of meteorological data. Our final selection was based on the Silhouette value, Dunn’s partition coefficient and Kaufman’s partition coefficient (Figure 2) for each cluster. These three parameters helped us choose the appropriate number of clusters, Kaufman and Rousseeuw [40] described their calculation process. When the silhouette value and Dunn’s partition coefficient show high values and Kaufman’s partition coefficient shows a low value, the calculated number of clusters can be considered as optimal. As shown in Figure 2, the optimal number of clusters was 2, independently of the meteorological dataset used. Consequently, in the following we divide the QTP in two clusters.

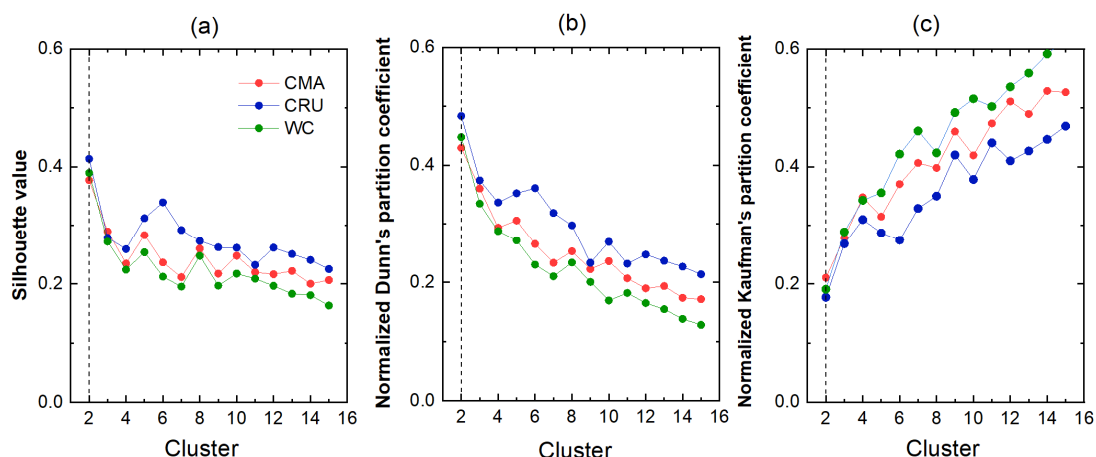


Figure 2. Average silhouette value (a) normalized Dunn’s partition coefficient (b) and normalized Kaufman’s partition coefficient (c) using each meteorological database across the QTP.

The fuzzy membership degree of each measuring station in each cluster was greater than 0.1. Therefore, the previous recommendation that the membership degree is at least 0.1 [12] could not be adopted in this study. Through numerical debugging of fuzzy membership degree, based on the analysis of the moisture source and distribution of precipitation in QTP, the minimum membership degree selected in this paper was 0.3. In other words, when the membership of each station in a cluster was greater than 0.3, the station was included in the cluster in order to calculate the regression equation. Multiple regression models were calculated using meteorological data of each region, and then they were inversely sorted from high to low according to the adjusted R^2 value. When the difference between the adjusted R^2 value of two sets of models was small, the one with the smaller number of meteorological parameters was selected for the final calculation (Table S1 in the supplemental material).

The optimal regression equation was used to calculate the fuzzy clustering equation of each month. The simulation value of each clustering regions was then generated by superposition, according to the

residual interpolated by the observation station. Finally, the two clustering results were superimposed according to the weight distribution to generate the final monthly isoscape.

2.5. Assessment Method

The coefficient of determination (R^2)

$$R^2 = \frac{\sum_{i=1}^n (\delta_i^M - \overline{\delta^O})^2}{\sum_{i=1}^n (\delta_i^O - \overline{\delta^O})^2} \quad (3)$$

with δ_i^O the observations, δ_i^M the simulation results, and $\overline{\delta^O}$ is the mean value of the observations, was used to evaluate the applicability of the two sets of simulated data in the QTP. The higher the R^2 value, the smaller the dispersion between the simulated and the observed values, the better the linear relationship, and the estimated value was closer to the measured value on the trend.

In addition, the leave-one-out ($n - 1$) “jackknife” resampling procedure [41] was applied in order to test the precipitation isoscape of the QTP with fuzzy clustering. The jackknife method tests the accuracy of simulation results by being applied for n number of iterations, in each iteration keeping the value of one station out of the model calculation procedure. Thus, it provides a measure of the accuracy of the simulation of the station.

3. Results and Analysis

3.1. Assessment of Previous Global Products in the QTP

Figure 3 shows the observed and estimated $\delta^{18}\text{O}$ values derived from the two global isoscapes on a monthly basis; the frames mark the summer half year from May to September when precipitation is mainly concentrated. More information about the R^2 values are provided as Table S2 in the supplementary material. Generally, the simulated intra-annual trends of OIPC and RCWIP are similar for most stations; although $R^2 > 0.8$ can be seen in many stations, weak performances do exist for some stations. The R^2 values ranged from 0.002 to 0.999 for OIPC and from 0.020 to 0.944 for RCWIP; the mean levels were 0.500 ± 0.274 and 0.434 ± 0.306 , respectively. Approximate 59% and 44% of stations in OIPC and RCWIP showed R^2 values higher than 0.5.

Because of the uneven intra-annual precipitation amount and the relatively weak availability of samples in the winter half year, not every station in Figure 3 has a 12 month time series. Regarding the OIPC simulation during the summer half year (Table S2 in supplementary material), the stations with high R^2 values (>0.9) were located in the southeast QTP (Larzi, Bomi, Nagqu, Cona and Baidi). Their altitudes ranged between 4000 and 4700 m a.s.l., all being higher than the average altitude of all 32 stations, with the exception of the Bomi station, located at 2737 m a.s.l. Regarding their moisture regime, these stations are mainly in the monsoon domain, except for the Cona station, located in the transition region. It should be mentioned that the global isoscape simulations greatly depend on the isotopic input from the GNIP data, and only one station, Lhasa, was included in the GNIP; the above-mentioned stations are generally close to the Lhasa station, both in terms of distance and of altitude, which may partly explain why the measurements of these stations show the best agreement with OIPC simulations. However, for RCWIP, the spatial distribution of R^2 seems different from that of OIPC, and some westerly dominated stations also showed high R^2 values. In general, there are obvious regional differences in the simulations of the two models OIPC and RCWIP, and a better predicted isoscape is still needed for the QTP.

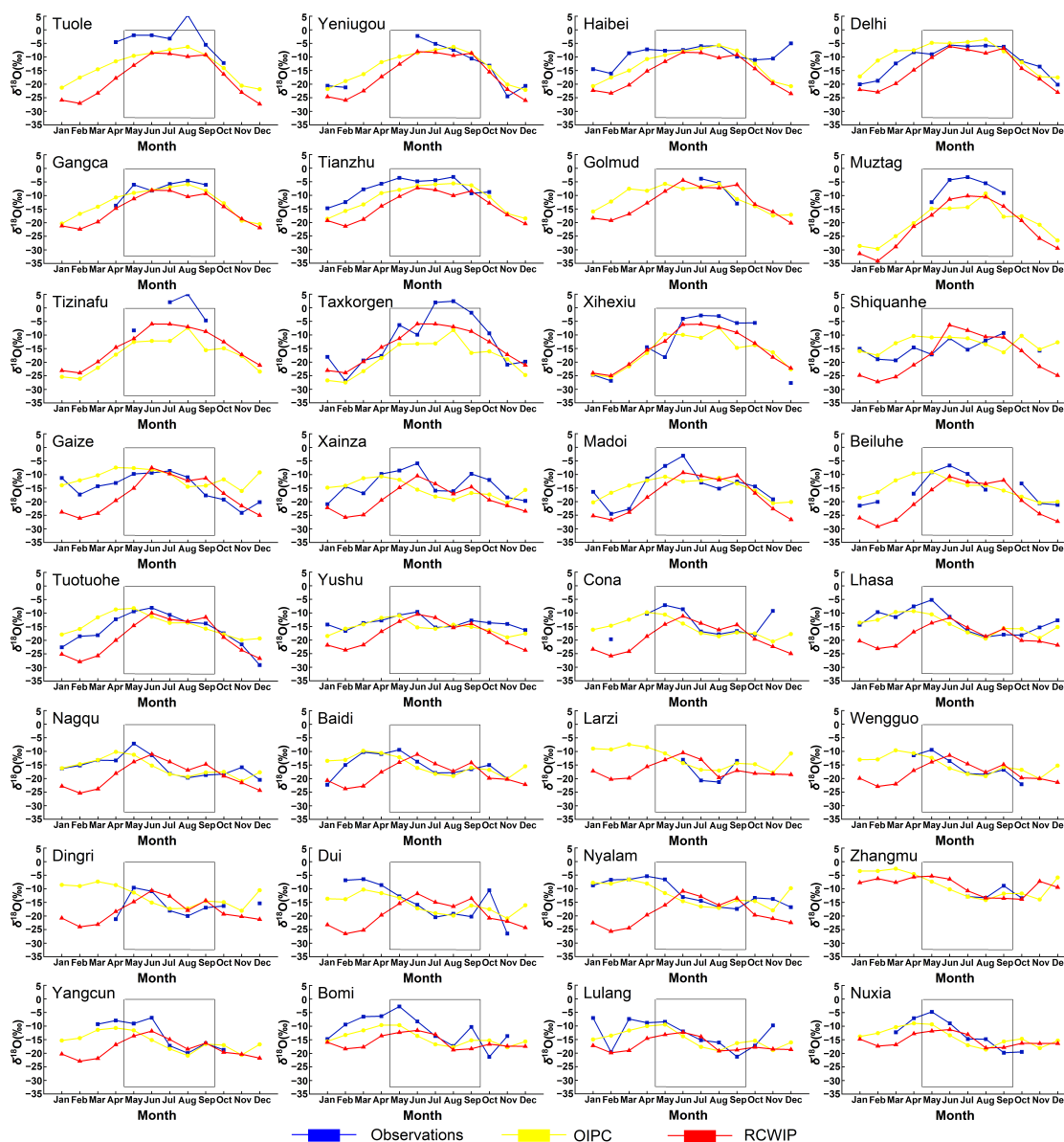


Figure 3. Monthly variations of observed and simulated $\delta^{18}\text{O}$ values at 32 stations across the QTP. The frame indicates the summer half year.

The isotopic data of each month in Figure 3 are multi-year averages, and the inter-annual variation is logically ignored. Here we selected the Lhasa station [13,16,29] to check the possible impact of the inter-annual variations. Although the isotopic observations in Lhasa shown in Figure 4 is still discontinuous in past decades, it does provide an available reference on the inter-annual issue of precipitation isotopes of the QTP. The $\delta^{18}\text{O}$ values show interannual fluctuations for all months; extreme values appear in some years, which can be seen in March and October. During the winter half year, with less samples, $\delta^{18}\text{O}$ simulations in Lhasa deviate significantly from the observed values. What may be the cause of interannual $\delta^{18}\text{O}$ value fluctuation in precipitation? Gao et al. [42,43] found that the interannual variation of $\delta^{18}\text{O}$ in summer precipitation in Lhasa was affected by the ENSO (El Niño-Southern Oscillation), and there was no significant correlation to the local precipitation amount and surface temperature. According to Figure 4, the simulated values of both global isoscapes were close to the observed multi-year average, especially for the summer half year. However, when strong ENSO events occurred, the representativeness of the long-term mean may have been needed to be considered.

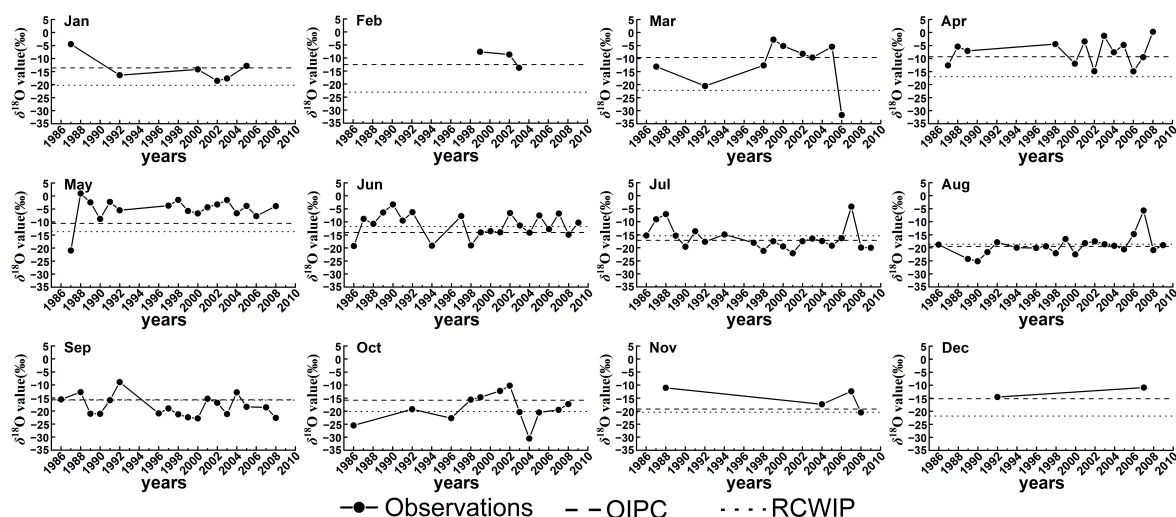


Figure 4. Comparison of monthly $\delta^{18}\text{O}$ simulated by Online Isotopes in Precipitation Calculator (OIPC) and Regionalized Cluster-based Water Isotope Prediction (RCWIP) and observed in Lhasa from 1986 to 2009.

3.2. Isoscape Established Using a Regionalized Clustering

3.2.1. Climate Clustering

Figure 5 presents the distribution of a fuzzy cluster membership across the QTP using the three meteorological datasets comprising CMA, CRU, and WC. Whichever dataset is applied, the fuzzy cluster analysis always went to two clusters; the spatial distribution of the two clusters across the QTP was generally the same, independently of the meteorological input. The first cluster (Figure 5a–c) was concentrated in the northwest region and in the Qilian mountain area in the northeast corner; the second (Figure 5d–f) was in the southeast region and in the Qaidam basin area. Therefore, in this paper, WC dataset were selected for calculation when establishing the new isoscape of the QTP.

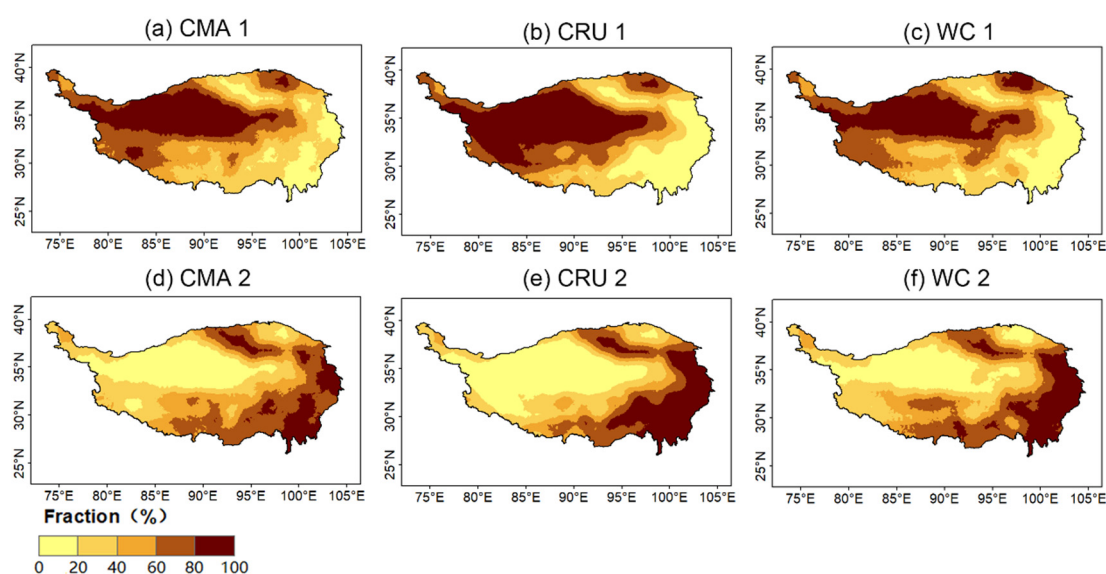


Figure 5. Maps showing the membership fraction of each cluster using the three climatological databases (CMA, CRU, and WC). Subfigures (a–c) show cluster 1, and (d–f) are cluster 2.

3.2.2. Establishing the Isoscape

Selecting the optimal regression model is a prerequisite for establishing an accurate isoscape. Using the data from 32 sampling stations in the QTP, we established a regional isoscape of stable oxygen isotopes in precipitation (Figure 6). In Figure 6, various spatial pattern of precipitation isotopes can be seen, indicating the different controlling regimes for each monsoon or season; the specific regions with high and low isotope values move all year round. From January to April, the high $\delta^{18}\text{O}$ value region gradually expanded from south to east; the eastern plateau experienced the $\delta^{18}\text{O}$ enriching process, while the northwestern Qinghai-Tibet Plateau was always a low $\delta^{18}\text{O}$ area. The monthly isoscapes between May and June showed significant changes. In May, the $\delta^{18}\text{O}$ values were higher at the southern and eastern regions, but lower at the western regions; in June, however, $\delta^{18}\text{O}$ was higher in the northwest and northeast regions and lower in the south. The moisture transported by the monsoon gradually strengthens, and the role of the westerlies' moisture becomes weak, resulting in a large regional change of $\delta^{18}\text{O}$. From July to September, the $\delta^{18}\text{O}$ value of precipitation on the QTP showed a spatial distribution with values lower in the south and higher in the north, and the northern plateau showed a relatively stable situation. In October, the areas with low $\delta^{18}\text{O}$ values in the central and southern parts of the QTP gradually decreased, and the $\delta^{18}\text{O}$ values increased. In November and December, the $\delta^{18}\text{O}$ value showed a spatial distribution of high values in the southeast and low values in the northwest.

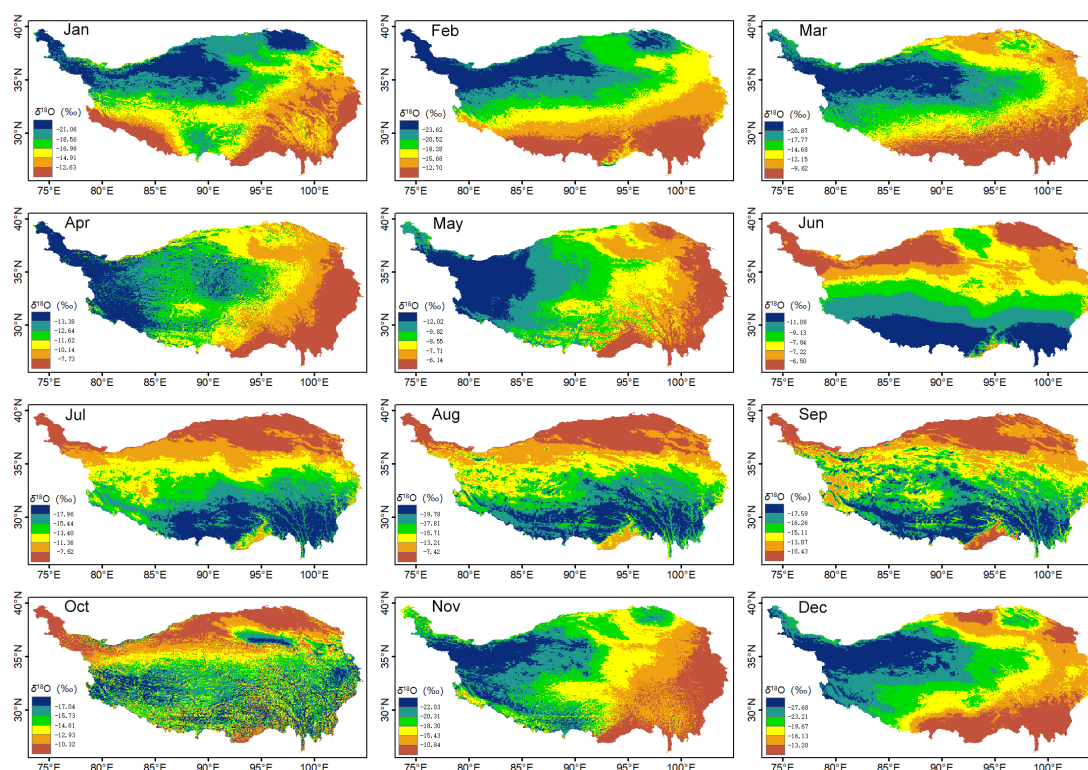


Figure 6. Monthly isoscape of stable oxygen isotopes in precipitation across the QTP.

3.2.3. Comparison with the OIPC and RCWIP

The OIPC and RCWIP are two widely applied global isoscapes available online. They provide helpful simulation data especially for areas where precipitation isotope measurements are scarce or do not exist at all. However, because of the climate and landform of the QTP as well as the relatively few observational data used for the development of those two global isoscapes, we considered that the isoscape models can be further improved for this part of the world. Compared to the OIPC and RCWIP isoscapes, the basic isotopic characteristics in our new isoscapes were consistent both spatially and temporally. We tested the method using the “jackknife” resampling procedure and showed the

absolute residuals between the simulated values of the three isoscapes and the observed monthly values from the 32 stations (Figure 7). Generally, the residual values during the summer half year were smaller than those during the winter half year, which was consistent for the three isoscapes. Compared with the OIPC and RCWIP datasets, the residuals of the new isoscape we propose in the study were significantly smaller for every month, which can be identified from the box plots. In addition, the maximum absolute residual outlier of the OIPC, close to 16‰ (Figure 7a), occurred in December; the absolute residual outlier value of the RCWIP occurred in February and equaled approximately 20‰ (Figure 7b); however, for the new isoscape, the maximum outlier value of absolute residual, less than 14‰, appeared in October (Figure 7c). Generally, the absolute residuals of our isoscape, either average or median, were closer to 0 than were those of the two other isoscapes, supporting the argument that the new isoscape we propose performs better for the QTP.

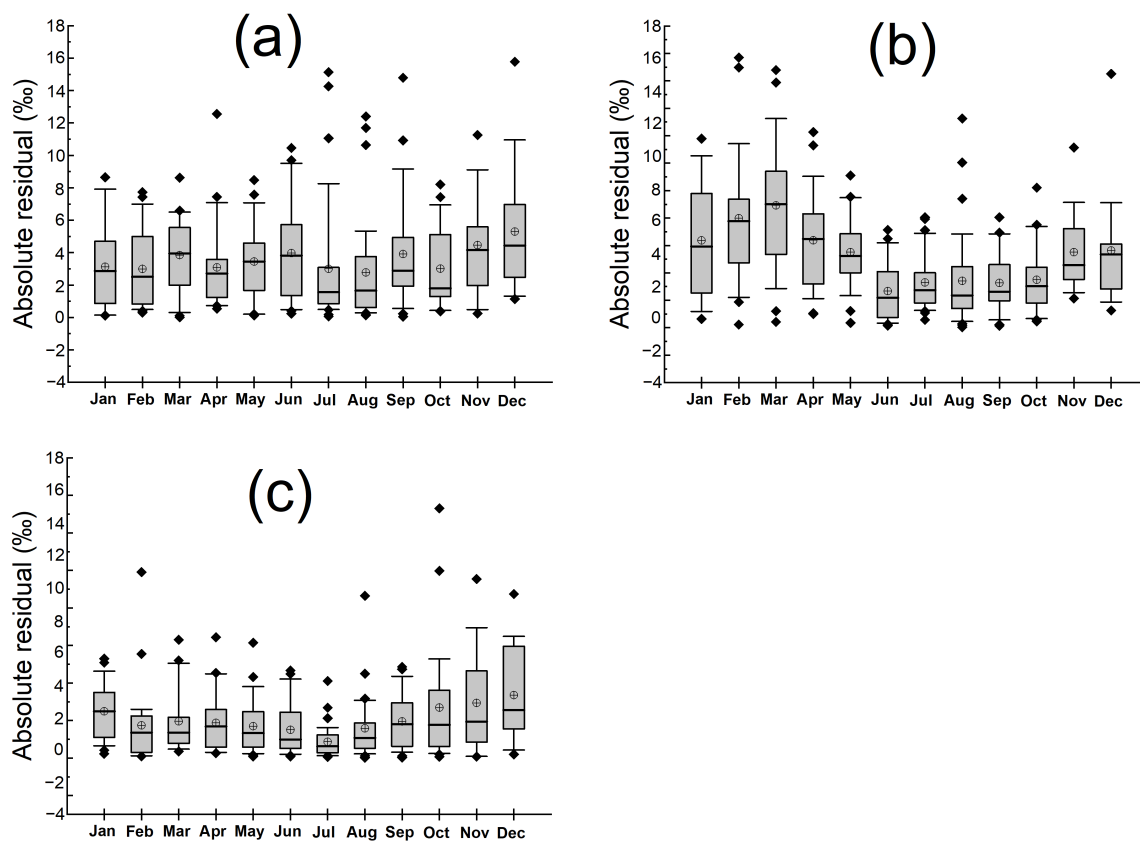


Figure 7. Box plots of the monthly distribution of absolute residuals between the three isoscapes and the observations at 32 stations: (a) OIPC, (b) RCWIP, and (c) this study. The boxes represent 25–75th percentiles, and the line through the box represents the median; the whiskers indicate the 90th and 10th percentiles; the rhombus above and below the whiskers indicates the outliers; and the circle with a cross in the center indicates the average number.

4. Conclusions

In this study, we evaluated the applicability of two sets of global precipitation isoscapes (OIPC and RCWIP) in the QTP. The results showed that the two isoscapes perform better for the summer half year than for winter, and the spatial incoherence of residuals can be seen for the two isoscapes. To create an improved isoscape using more observation input, we considered a regionalized fuzzy clustering method. According to the cross validation, our isoscape showed a better performance than the previous global isoscapes over the QTP, and the residuals greatly reduced in our new isoscape. To create a regional isoscape in many other regions in the future, the fuzzy cluster method can be reconsidered and recommended, especially for regions with complex controlling regimes of precipitation isotopes.

It should be noticed that the long-term averages are always effective for a specific year, and more in situ observations of precipitation isotopes are still of great importance.

Supplementary Materials: The following are available online at <http://www.mdpi.com/2073-4441/12/12/3392/s1>, Table S1: Regression factors applied for each month over the QTP. Table S2: The R^2 values of OIPC and RCWIP for each station over the QTP.

Author Contributions: Y.S. (Yudong Shi), S.W., and M.Z. performed background research and designed the study; Y.S. (Yudong Shi) and S.W. performed the data analyses and wrote the manuscript; A.A.A., R.G., Y.S. (Yang Song), and X.Z. contributed to data analysis and manuscript preparation. All authors have read and agreed to the published version of the manuscript.

Funding: This work was supported by the National Natural Science Foundation of China nos. 41701028 and 41971034, and the Scientific Research Program of Higher Education Institutions of Gansu Province no. 2018C-02.

Acknowledgments: The authors greatly thank Tandong Yao (Institute of Tibetan Plateau Research, Chinese Academy of Sciences) and his team for the Tibetan Network of Isotopes in Precipitation (TNIP) data. Many thanks also go to the other isotopic data providers involved in this study. We would like to acknowledge the IAEA for providing RCWIP product and Gabriel Bowen (University of Utah) for providing OIPC product.

Conflicts of Interest: The authors have declared no conflict of interest. The work described here has not been submitted elsewhere for publication, in whole or in part, and all the authors listed have approved the manuscript that is enclosed.

References

1. Bowen, G.J.; Cai, Z.; Fiorella, R.P.; Putman, A.L. Isotopes in the water cycle: Regional-to global-scale patterns and applications. *Annu. Rev. Earth. Planet. Sci.* **2019**, *47*, 453–479. [[CrossRef](#)]
2. Jasechko, S. Global isotope hydrogeology—Review. *Rev. Geophys.* **2019**, *57*, 835–965. [[CrossRef](#)]
3. Bowen, G.J. Isoscapes: Spatial pattern in isotopic biogeochemistry. *Annu. Rev. Earth. Planet. Sci.* **2010**, *38*, 161–187. [[CrossRef](#)]
4. Wang, S.; Zhang, M.; Bowen, G.J.; Liu, X.; Du, M.; Chen, F.; Qiu, X.; Wang, L.; Che, Y.; Zhao, G. Water source signatures in the spatial and seasonal isotope variation of Chinese tap waters. *Water Resour. Res.* **2018**, *54*, 9131–9143. [[CrossRef](#)]
5. Hollins, S.E.; Hughes, C.E.; Crawford, J.; Cendón, D.I.; Meredith, K.T. Rainfall isotope variations over the Australian continent—implications for hydrology and isoscape applications. *Sci. Total Environ.* **2018**, *645*, 630–645. [[CrossRef](#)] [[PubMed](#)]
6. Allen, S.T.; Kirchner, J.W.; Goldsmith, G.R. Predicting spatial patterns in precipitation isotope ($\delta^2\text{H}$ and $\delta^{18}\text{O}$) seasonality using sinusoidal isoscapes. *Geophys. Res. Lett.* **2018**, *45*, 4859–4868. [[CrossRef](#)]
7. Zhang, M.; Wang, S. A review of precipitation isotope studies in China: Basic pattern and hydrological process. *J. Geogr. Sci.* **2016**, *26*, 921–938. [[CrossRef](#)]
8. Bowen, G.J.; Wilkinson, B. Spatial distribution of $\delta^{18}\text{O}$ in meteoric precipitation. *Geology* **2002**, *30*, 315–318. [[CrossRef](#)]
9. Peng, P.; Zhang, X.J.; Chen, J. Bias correcting isotope-equipped GCMs outputs to build precipitation oxygen isoscape for eastern China. *J. Hydrol.* **2020**, *589*, 125153. [[CrossRef](#)]
10. Vander Zanden, H.B.; Nelson, D.M.; Wunder, M.B.; Conkling, T.J.; Katzner, T. Application of isoscapes to determine geographic origin of terrestrial wildlife for conservation and management. *Biol. Conserv.* **2018**, *228*, 268–280. [[CrossRef](#)]
11. Bowen, G.J.; Wassenaar, L.I.; Hobson, K.A. Global application of stable hydrogen and oxygen isotopes to wildlife forensics. *Oecologia* **2005**, *143*, 337–348. [[CrossRef](#)]
12. Terzer, S.; Wassenaar, L.I.; Araguás-Araguás, L.J.; Aggarwal, P.K. Global isoscapes for $\delta^{18}\text{O}$ and $\delta^2\text{H}$ in precipitation: Improved prediction using regionalized climatic regression models. *Hydrol. Earth Syst. Sci.* **2013**, *17*, 4713–4728. [[CrossRef](#)]
13. IAEA/WMO. Global network of isotopes in precipitation. the GNIP Database. 2020. Available online: <http://www.iaea.org/water> (accessed on 1 January 2020).
14. Lisowska-Gaczorek, A.; Cienkosz-Stepańczak, B.; Szostek, K. Oxygen stable isotopes variation in water precipitation in Poland—anthropological applications. *Anthropol. Rev.* **2017**, *80*, 57–70. [[CrossRef](#)]
15. Tian, Q.; Fang, X.; Wang, M. Sedimentary *n*-alkanes record of precipitation D/H ratios in arid regions of the Tibetan Plateau. *Chinese Sci. Bull.* **2017**, *62*, 700–710. (In Chinese)

16. Yao, T.; Masson-Delmotte, V.; Gao, J.; Yu, W.; Yang, X.; Risi, C.; Sturm, C.; Werner, M.; Zhao, H.; He, Y.; et al. A review of climatic controls on $\delta^{18}\text{O}$ in precipitation over the Tibetan Plateau: Observations and simulations. *Rev. Geophys.* **2013**, *51*, 525–548. [[CrossRef](#)]
17. Sun, C.; Chen, Y.; Li, J.; Chen, W.; Li, X. Stable isotope variations in precipitation in the northwesternmost Tibetan Plateau related to various meteorological controlling factors. *Atmos. Res.* **2019**, *227*, 66–78. [[CrossRef](#)]
18. Wu, H.; Li, X.; Zhang, J.; Li, J.; Liu, J.; Tian, L.; Fu, C. Stable isotopes of atmospheric water vapour and precipitation in the northeast Qinghai-Tibetan Plateau. *Hydrol. Process.* **2019**, *33*, 2997–3009. [[CrossRef](#)]
19. Zhang, T.; Zhang, Y.; Guo, Y.; Ma, N.; Dai, D.; Song, H.; Qu, D.; Gao, H. Controls of stable isotopes in precipitation on the central Tibetan Plateau: A seasonal perspective. *Quatern. Int.* **2019**, *513*, 66–79. [[CrossRef](#)]
20. Ren, W.; Yao, T.; Xie, S.; He, Y. Controls on the stable isotopes in precipitation and surface waters across the southeastern Tibetan Plateau. *J. Hydrol.* **2017**, *545*, 276–287. [[CrossRef](#)]
21. Gao, J.; Masson-Delmotte, V.; Yao, T.; Tian, L.; Risi, C.; Hoffmann, G. Precipitation water stable isotopes in the south Tibetan Plateau: Observations and modeling. *J. Clim.* **2011**, *24*, 3161–3178. [[CrossRef](#)]
22. He, Y.; Gao, J.; Yao, T.; Ding, Y.; Xin, R. Spatial distribution of stable isotope in precipitation upon the Tibetan Plateau analyzed with various interpolation methods. *J. Glaciol. Geocryol.* **2015**, *37*, 351–359. (In Chinese)
23. Xu, X.; Zhao, T.; Lu, C.; Guo, Y.; Chen, B.; Liu, R.; Li, Y.; Shi, X. An important mechanism sustaining the atmospheric “water tower” over the Tibetan Plateau. *Atmos. Chem. Phys.* **2014**, *14*, 11287–11295. [[CrossRef](#)]
24. Zhang, Y.; Li, B.; Zheng, D. Datasets of the boundary and area of the Tibetan Plateau. *Glob. Chang. Res. Data Publ. Repos.* **2014**. [[CrossRef](#)]
25. Ren, M.; Bao, H. *Natural Regions of China and Their Exploitation*; The Commercial Press: Beijing, China, 1992; pp. 1–483. (In Chinese)
26. Zhang, C.; Tang, Q.; Chen, D. Recent changes in the moisture source of precipitation over the Tibetan Plateau. *J. Clim.* **2017**, *30*, 1807–1819. [[CrossRef](#)]
27. Li, Z.; Yao, T.; Tian, L.; Xu, B.; Wu, G. Variations of $\delta^{18}\text{O}$ in precipitation from the Muztagata Glacier, East Pamirs. *Sci. China Ser. D* **2006**, *49*, 36–42. [[CrossRef](#)]
28. Zhao, L.; Yin, L.; Xiao, H.; Cheng, G.; Zhou, M.; Yang, Y.; Li, C.; Zhou, J. Isotopic evidence for the moisture origin and composition of surface runoff in the headwaters of the Heihe River basin. *Chinese Sci. Bull.* **2011**, *56*, 406–415. [[CrossRef](#)]
29. Liu, J.; Song, X.; Yuan, G.; Sun, X.; Yang, L. Stable isotopic compositions of precipitation in China. *Tellus B* **2014**, *66*, 22567. [[CrossRef](#)]
30. Wu, H.; Li, X.; Jiang, Z.; Li, J.; Zheng, X.; Zhao, D. Variations in water use for *achmatherum splendens* in Lake Qinghai Watershed, based on δD and $\delta^{18}\text{O}$. *Acta Ecol. Sinica* **2015**, *35*, 8174–8183. (In Chinese)
31. Gui, J.; Li, Z.; Feng, Q.; Wei, W.; Li, Y.; Lü, Y.; Yuan, R.; Zhang, B. Space-time characteristics and environmental significance of the stable isotopes in precipitation in the Gulang River basin. *Environ. Sci.* **2019**, *40*, 149–156. (In Chinese)
32. Zhu, J.; Chen, H.; Gong, G. Hydrogen and oxygen isotopic compositions of precipitation and its water vapor sources in Eastern Qaidam Basin. *Environ. Sci.* **2015**, *36*, 2784–2790. (In Chinese)
33. Sun, C.; Shen, Y.; Chen, Y.; Chen, W.; Liu, W.; Zhang, Y. Quantitative evaluation of the rainfall influence on streamflow in an inland mountainous river basin within Central Asia. *Hydrol. Sci. J.* **2018**, *63*, 17–30. [[CrossRef](#)]
34. Ren, W.; Yao, T.; Yang, X.; Joswiak, D.R. Implications of variations in $\delta^{18}\text{O}$ and δD in precipitation at Madoi in the eastern Tibetan Plateau. *Quatern. Int.* **2013**, *313*, 56–61. [[CrossRef](#)]
35. Yang, Y.; Wu, Q.; Yun, H. Characteristic analysis of stable isotope variation in precipitation and rivers in Beilu river permafrost region. *Adv. Water Sci.* **2013**, *24*, 978–985. (In Chinese)
36. Cui, J.; Tian, L.; Biggs, T.W.; Wen, R. Deuterium-excess determination of evaporation to inflow ratios of an alpine lake: Implications for water balance and modeling. *Hydrol. Process.* **2017**, *31*, 1034–1046. [[CrossRef](#)]
37. Zhao, Y.; Zhu, J.; Xu, Y. Establishment and assessment of the grid precipitation datasets in China for the past 50 years. *J. Meteorol. Sci.* **2014**, *34*, 414–420. (In Chinese)
38. New, M.; Lister, D.; Hulme, M.; Makin, I. A high-resolution data set of surface climate over global land areas. *Clim. Res.* **2002**, *21*, 1–25. [[CrossRef](#)]
39. Fick, S.E.; Hijmans, R.J. WorldClim 2: New 1-km spatial resolution climate surfaces for global land areas. *Int. J. Climatol.* **2017**, *37*, 4302–4315. [[CrossRef](#)]

40. Kaufman, L.; Rousseeuw, P.J. *Finding Groups in Data: An Introduction to Cluster Analysis*; John Wiley & Sons: New York, NY, USA, 1990; pp. 1–342.
41. Wu, C.F.J. Jackknife, bootstrap and other resampling methods in regression analysis. *Ann. Stat.* **1986**, *14*, 1261–1295. [[CrossRef](#)]
42. Gao, J.; Masson-Delmotte, V.; Risi, C.; He, Y.; Yao, T. What controls precipitation $\delta^{18}\text{O}$ in the southern Tibetan Plateau at seasonal and intra-seasonal scales? A case study at Lhasa and Nyalam. *Tellus B* **2013**, *65*, 21043. [[CrossRef](#)]
43. Gao, J.; He, Y.; Masson-Delmotte, V.; Yao, T. ENSO effects on annual variations of summer precipitation stable isotopes in Lhasa, southern Tibetan Plateau. *J. Clim.* **2018**, *31*, 1173–1182. [[CrossRef](#)]

Publisher's Note: MDPI stays neutral with regard to jurisdictional claims in published maps and institutional affiliations.



© 2020 by the authors. Licensee MDPI, Basel, Switzerland. This article is an open access article distributed under the terms and conditions of the Creative Commons Attribution (CC BY) license (<http://creativecommons.org/licenses/by/4.0/>).